Hindawi
Geofluids
Volume 2022, Article ID 2373133, 15 pages
https://doi.org/10.1155/2022/2373133

Research Article

Researches on the Excavation Disturbance of Shield Tunnel in Sandy Cobble Ground

Wei Wang,[1] Jingjing Liu,[1] Xueming Zhang,[2] and Jing Chen[2]

[1]*China Hebei Construction and Geotechnical Investigation Group Ltd., Shijiazhuang 050227, China*
[2]*School of Civil Engineering, Beijing Jiaotong University, Beijing 100044, China*

Correspondence should be addressed to Jing Chen; 20121024@bjtu.edu.cn

Received 10 April 2022; Accepted 28 May 2022; Published 14 June 2022

Academic Editor: Di Feng

The sandy cobble ground has loose structure, uneven particle size, and random distribution characteristics, which may lead to the local collapse of ground. This paper carried out field tests based on the project of Luoyang urban rail transit. For this, the surface settlement, pore water pressure, and earth pressure in the test section were measured. The excavation disturbance and influence range on the soil layer in each stage of earth pressure balance shield tunneling were studied. Meanwhile, based on the key construction elements in sandy cobble ground, a numerical simulation method was proposed based on shield construction parameters. The disturbance characteristics of deformation, seepage action, and stress state of the sandy cobble ground during shield construction were obtained through numerical calculation. The rationality of the simulation results was verified by the measured tests. The results showed that the measured data were in good agreement with the simulation results. The research results provide a calculation method for predicting the soil disturbance in the earth pressure balance shield construction in a sandy cobble ground.

1. Introduction

The earth pressure balance shield method has been widely utilized in sandy cobble ground. Sandy cobble ground has the characteristics of loose structure and poor self-stability. The constitutive model of geotechnical material based on the thermodynamic process of porous granular material and its numerical calculation method is of great significance to study the influence of shield tunneling on the disturbance of stratum [1, 2]. The sandy cobble ground shows strong instability from the mechanical mechanism [3, 4], which brings severe challenges to the application of shield construction. Under complex ground condition and external environment, how to deal with the coupling of multiphysical fields in the construction process is an important issue [5, 6]. In fact, there are complex physical-chemical effects between the rich groundwater and mineral particles in the pores [7–9]. Therefore, the disturbance during shield tunneling destroys the original relatively stable state, resulting in collapse or uplift, greater ground loss, and even local ground failure [10–12]. However, there exist many difficulties in constructing shield tunnel in sandy cobble ground. Among them, the soil pressure, tunneling rate, grouting pressure, and other construction parameters have great disturbances to the soil [13–15], so the whole construction process has a great impact on the soil layer. The influence of disturbance is of great significance to the safety of various facilities and surrounding buildings.

Coupled with the complexity of the shield construction parameters, it is easy to cause instability of excavation surface during shield construction [16–18]. A cavity is formed in the upper ground of the shield tunneling area. Later, under the combined action of ground load and mechanical vibration, the ground has a large settlement or even collapses. The tunnel section is partially frozen during shield construction, and construction parameters such as shield thrust, cutter head torque, and grouting pressure are significantly different. When the shield machine is located in the frozen soil layer, the shield machine deforms under the influence of the frozen soil force, which causes the deformation of the tunnel cross section. Hence, the tunnel segment bears great pressure, and even cracks appear. At the same

time, the external force/high temperature generated during shield tunneling melts the soil around the shield [19] and leads to the migration of soil solid particles [20].

In addition, some tunnels pass through polluted factory production areas. These areas are seriously polluted, which has brought great challenges to subway construction. At the same time, the water-rich sandy cobble ground has a loose structure, large porosity, and high permeability. Due to tunnel construction, the water within a certain range around the tunnel is affected by excavation disturbance, resulting in the change of microstructure characteristics and the migration of pollutants [21, 22].

Most researches on the earth pressure and excess pore water pressure generated by shield construction on the surrounding soil are mainly concentrated on various soil types such as silt, loess, and clay [23–25], and there is little measured data on sandy cobble ground. This paper is concentrated on the construction project of Luoyang urban rail transit. The project area is covered by a quaternary system, which is composed of silty clay, silty sand, and sandy cobble ground. According to the characteristics of sandy cobble ground, through numerical analysis and field test, the deformation law and stress state change of the ground when the shield passes through sandy cobble ground are revealed, and the reasonable selection of control measures when shield passes through sandy cobble ground is provided.

2. Field Test

The Suitang station of the construction project of Luoyang urban rail transit was selected for field test, which is sensitive to land subsidence caused by precipitation. This station is located in the botanical garden on the east side of Wangcheng avenue in Luoyang city and is arranged along the planned north-south direction (Figure 1). Meanwhile, the groundwater level in the construction area is high. To discuss the surface deformation and earth pressure caused by soil disturbance, deformation and stress sensors are arranged in front and above of shield tunnel to test the deformation and stress state of surface during construction process. Eight typical sections were selected for testing. The width of the test section includes the whole width of the upward (left line) and downward (right line) shield tunnels and extends to both sides beyond the influence range.

Three surface settlement monitoring sections D1-D3 were set up in the test section. The surface settlement test uses a high-precision level instrument to test the settlement and its change with time when it reaches and leaves the area. Two ground settlement monitoring sections D4-D5 are set to monitor ground settlement. Ground settlement using ABS settlement pipe (the diameter is 53 mm) is buried by drilling method. There are 6 settling magnetic rings at the top of the central line of the up or down tunnels and 12 settling magnetic rings between the central lines of the up or down tunnels.

Three monitoring sections of earth pressure and pore water pressure are set up from D6 to D8, which are perpendicular to the direction of tunnel excavation. The earth pressure gauge is used to measure the stress in the soil layer facing the direction of the tunnel during tunneling, and the pore water pressure gauge is used to measure the change of pore water pressure in the ground during many engineering construction process [26–29]. During the burying process, the sensor is fixed on a special fixed bracket, and the sensor is placed in the borehole with a set depth through the guide rod. Four measurement holes are set for each section, which are located on the central axis of the up and down tunnels, the central line of the distance between the two tunnels, and the side line of the tunnel. The sensor is set in front of the central line of the tunnel. The earth pressure gauge is arranged from the surface to the depth direction, and five measuring points are set for each measuring hole. The buried depths are 6, 8, 10, 13, and 16 m. The pore water pressure gauge is arranged from the surface to the depth direction, and three measuring points are set for each measuring hole. The buried depths are 10, 13, and 16 m.

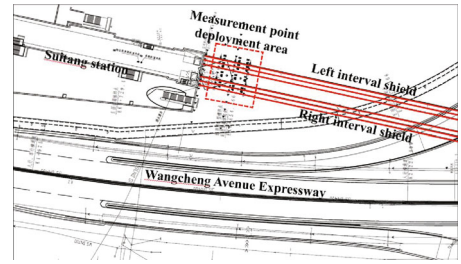

Figure 1: Shield tunnel measurement field layout.

3. Numerical Simulation of Shield Tunnel Construction

3.1. Physical Model and Boundary Conditions. Abaqus finite element software was used for modeling, which is mature and can better simulate the on-site environment of the construction area [30–32]. The diameter of the double-track circular tunnel is 6.4 m. Considering the boundary effect on the simulated excavation, the calculated size of the model is taken as 85 m × 159 m × 50 m, as shown in Figure 2. The model includes four parts: soil, shield machine, segment, and other generation layers. The model has 160, 775 elements and 231, 679 nodes. The left line tunnel excavation depth is 58.5 m, the right line tunnel excavation depth is 45 m, and the excavation is carried out at 1.5 m per ring. The left tunnel excavates 39 loops, and the right tunnel excavates 30 loops. To reduce the boundary effect on the model, the model adopts homogeneous boundary conditions, and the same displacement constraints are imposed on the left and right sides in the X direction and the front and back sides in the Y direction, respectively. The upper boundary (ground surface) of Z is a free boundary, and the lower boundary is a fixed boundary. In the pore water pressure dissipation/stress coupling analysis besides the normal load and displacement boundary conditions, it is necessary to set the corresponding load and boundary conditions for the pore water pressure. The pore water pressure is set at the drainage boundary at 9 m below the ground surface.

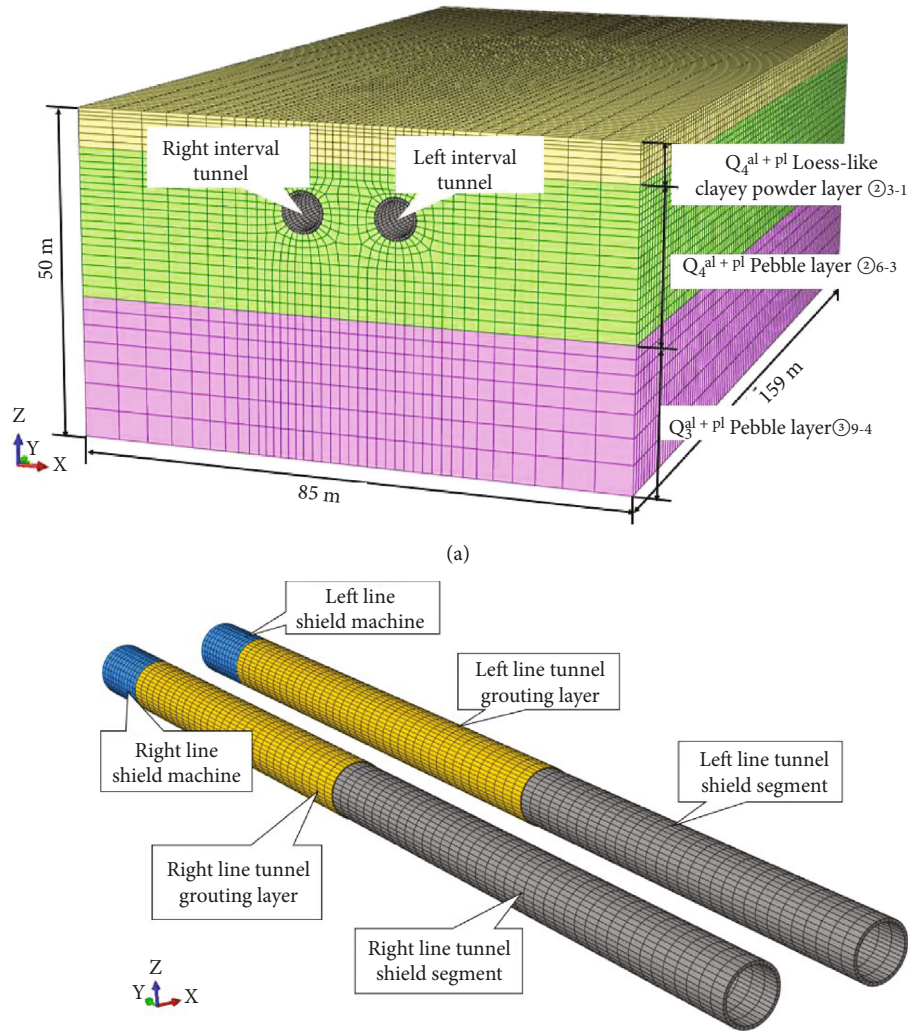

Figure 2: Calculation model: (a) soil layers and (b) segment.

3.2. Physical and Mechanical Parameters. The test results show that due to the large internal friction angle of sandy cobble ground, the failure criterion of the Mohr-Coulomb theory can better reflect the shear failure process of actual geomaterials. Combined with the suggested results of the mechanical parameters of each soil layer in the geotechnical engineering survey report, the main parameters of the ground are shown in Table 1. Both the shield shell and the tube sheet ring adopt the isotropic elastic material constitutive. The elastic modulus and Poisson ratio of the shield shell material are taken with reference to the parameters of the steel. Due to the heavy weight of the shield machine head, it is converted into the density of steel. The lining is poured with C50 concrete, and the segmented segment ring is considered as a homogeneous ring. Since the lining ring is formed by the staggered joints of multiple segments, the effective efficiency of bending stiffness $\eta = 0.85$ is introduced considering the influence of joint on ring stiffness.

The shield construction produces a shield tail gap, which is composed of the volume occupied by the thickness of the shield shell, the reserved lining installation clearance, and the overexcavation clearance. In the numerical simulation, the shield tail gap is extended to an equivalent layer with uniform thickness to simulate the influence of formation loss. According to the measured data on site, the size of the shield tail gap is about 60 mm. Due to the high permeability of sandy cobble ground, it is difficult to guarantee the quality of grouting. This paper simulates the thickness of the shield tail gap as 120 mm. To simulate the mechanical properties of the grouting material at different stages, linear elastic materials are used to simulate the property changes of the single-liquid active slurry.

During the solidification stage, the elastic modulus of the slurry increases slowly during fluid solidification, and the increase in the elastic modulus of the slurry during plastic solidification is more obvious. According to the actual solidification process of synchronous grouting material at the tail of shield, the simulation is divided into three cases [33–35]. When the liquid grouting material is separated from the shield shell, the elastic modulus of the so-called equivalent layer is 0.5 MPa. For short-term solidified grouting material,

Table 1: Calculation parameters.

Soil layer	Density (g/cm^3)	Elastic modulus (MPa)	Poisson's ratio	Cohesion (kPa)	Internal friction angle (kPa)	Permeability coefficient (m/s)
Clay	1.81	6.13	0.3	21	20	1.74×10^{-5}
Cobble	2.2	55	0.23	1	42	1.62×10^{-3}
Cobble	2.2	60	0.23	2	42	1.62×10^{-3}

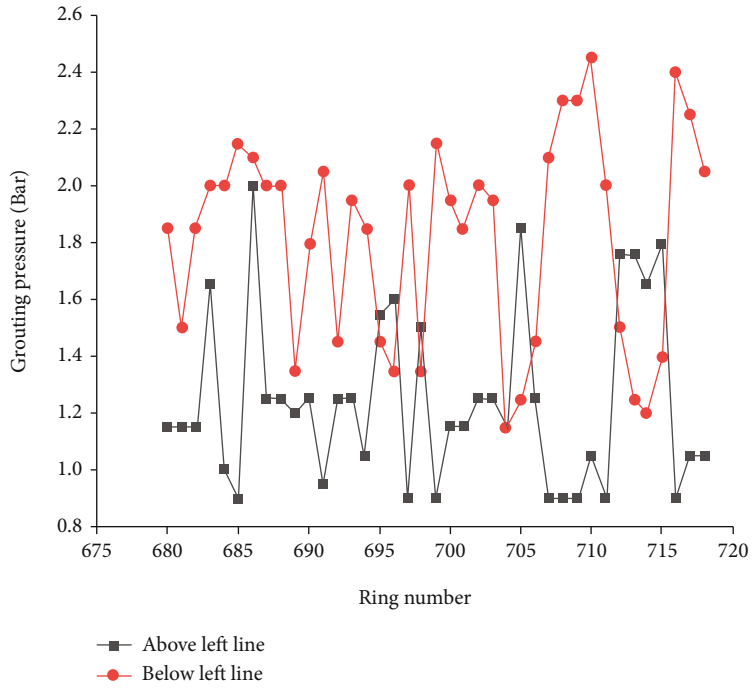

Figure 3: Measured results of grouting pressure on the left line.

the elastic modulus is taken as 4 MPa. For long-term solidified grouting material, the elastic modulus is taken as 400 MPa.

This paper mainly considers the influence of the excavation surface support pressure and grouting pressure on the stresses and deformations of the ground during the construction of the shield tunnel. After the shield tail passes through the section, the grouting pressure dissipates in a short time and reaches uniformity [36, 37]. As the grout solidifies, the grouting pressure disappears, and the grout begins to withstand the water and earth pressure in the formation and is transferred to the lining. Based on this, it is determined that the grouting pressure in the finite element simulation is only the time after the shield tail is separated from the ring segment. With the shield advances, the grouting pressure disappears. The distribution form of grouting pressure usually has the uniform grouting form uniformly distributed in the whole ring and the distribution form considering gravity. Through the simulation analysis of shield tunnel excavation under several different grouting pressure distribution forms, it is found that the nonuniform grouting form considering the influence of gravity is roughly consistent with the measured values. In addition, the field measured data shows that the grouting pressure on the upper part of the outer ring of the segment is the smallest, and the grouting pressure in the lower part is the largest, which is linearly distributed from top to bottom. Therefore, this simulation uses nonuniform distribution to act on the periphery of the pipe segment and the inner surface of the soil, and the upper and lower grouting pressure results are consistent with the measured data (Figure 3). In the process of shield construction, the chamber earth pressure is the construction control parameter. This simulation approximates that the chamber earth pressure is equal to the front thrust, which acts on the circular excavation surface. The result of the size is determined according to the field measured data (Figure 4).

3.3. Numerical Simulation Method. Pore water pressure mainly occurs in the upper sandy cobble ground. The aquifer is mainly a very strong water-rich ground. Therefore, fluid structure coupling analysis should be carried out in numerical simulation. The numerical simulation adopts the direct coupling method, and the analysis results are obtained by using the coupling element of displacement and pore water pressure. This coupling method is realized by calculating the element matrix or element load of displacement and pore water pressure. The fluid-solid coupling problem is

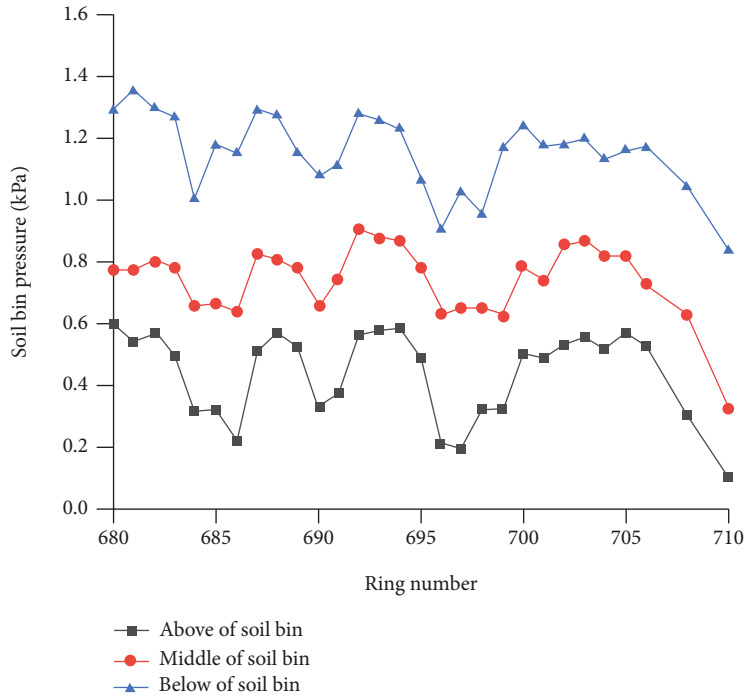

Figure 4: Measured result of soil pressure on the left line.

saturated seepage problem; that is, the soil layer below the groundwater is considered to be saturated. The finite element mesh is fixed on the soil skeleton, and gas or liquid can flow through the mesh, but the continuity equation of the fluid needs to be satisfied. The Biot's theory was used to calculate the mechanical properties of the soil, and Forchheimer's permeability law was used to simulate liquid permeability [38]. In addition, this discussion focuses on the distribution of excess pore water pressure as well as the dissipation process under the fluid-structure coupling effect.

Shield tunnel is usually studied as a discontinuous process [39, 40]. The forward movement of shield is actually the migration of shield stiffness and load. The method of unit activation and removal is used to deal with the change of unit stiffness. When the excavation surface advances forward, the shield head gradually deepens, and the shield tail gradually comes out, which may cause damage to the surrounding engineering environment [41, 42]. When the shield moves forward, other structures connected to the shield must also move forward simultaneously. The length of each forward advance is the width of segment unit, and the unit material is changed at the same time.

4. Stratum Deformation and Stress Distribution

4.1. Tunnel Surface Settlement. During the tunneling process of the shield machine, the soil disturbance gradually spreads to the lateral sides, resulting in a funnel area on the top of the tunnel. Shield tunneling not only causes the settlement of the ground directly above the tunnel, but also causes the settlement of the soil layer around a certain range of the axis; the calculated surface settlement is shown in Figure 5. From Figure 5, after the left line shield excavation is completed, the finite element macroscopic simulation of the sandy cobble ground surface lateral settlement takes on a classic Gauss curve distribution proposed by Peck formula, and the surface settlement at the top of the tunnel takes on a V shape. The maximum values occurred at the center axis of the tunnel, and the ground surface within twice the tunnel diameter had obvious subsidence. When the excavation of the right line tunnel is completed, the surface settlement on the two tunnels takes on a W shape.

The use of the Peck formula is based on the results of two important parameters, i.e., the width of the settlement trough as well as the formation loss rate. The Gauss method is used to fit the measured data and the simulated results. The goodness of fit of the measured results $R^2 = 0.9860$, and the goodness of fit of the simulation results $R^2 = 0.9990$, states clearly that the Gauss method has a better simulation effect. Finally, the average result of the simulation result of settlement trough width i is 5.6 m, which is slightly larger than the average result of the measured result of 3.31 m. The settlement tank width is much narrower than that of general clay and sand. The calculated maximum settlement S_{max} is 12.84 mm, which is basically the same as the average measured result of 11.28 mm.

Research results show that the surface settlement induced by shield tunnel excavation can be defined into five stages according to time: (a) initial settlement, (b) excavation surface settlement (or uplift), (c) through settlement, (d) tail joint settlement, and (e) subsequent consolidation settlement. Figure 6 shows the comparison of settlement duration curves of typical monitoring points. The settlement curve trend of the six observation points is roughly the same.

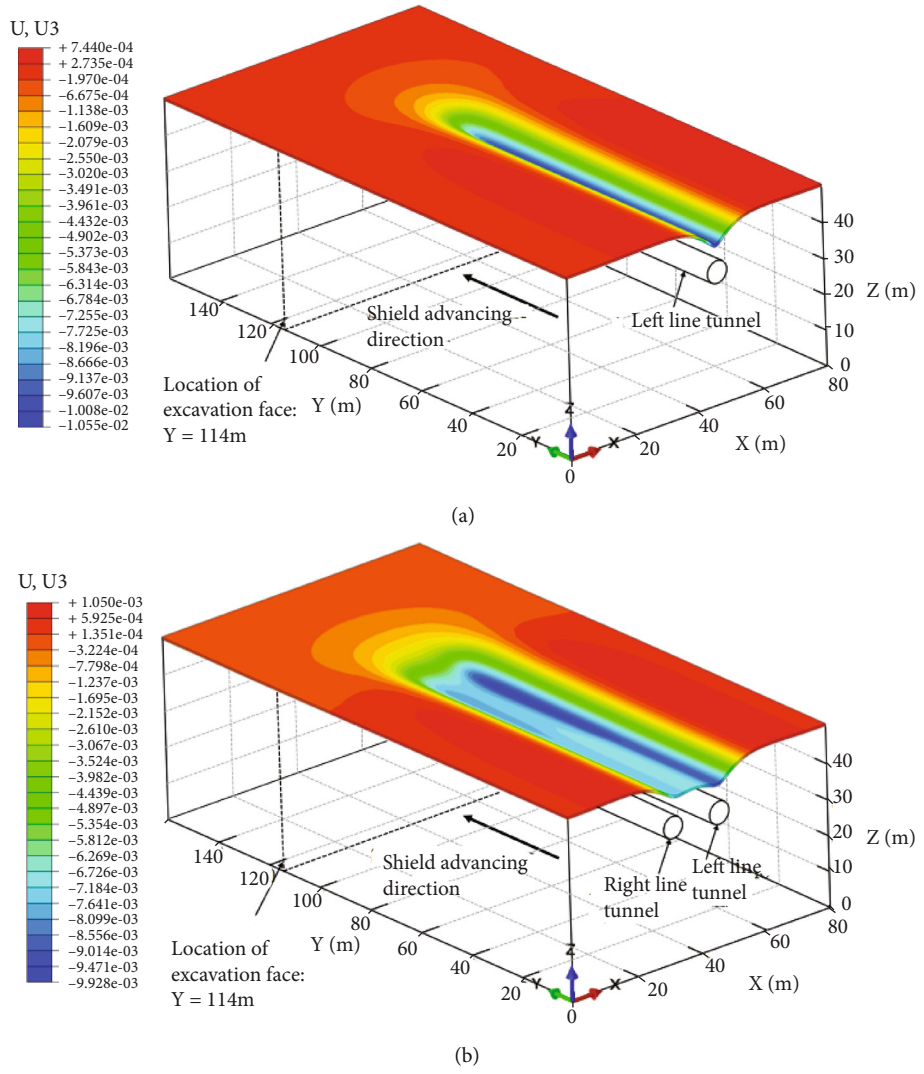

Figure 5: Surface settlement on: (a) left line and (b) right line.

However, the sandy cobble ground has loose structure, uneven particle size, irregular cobble distribution, and almost zero cohesion. Therefore, it has the characteristics of high sensitivity and force sensitivity. The destruction of sandy cobble ground is sudden, and the stability time after destruction is relatively short. Therefore, compared with clay layer, there is no obvious creep deformation stage.

Figure 6 shows that the simulation results are nearly consistent with the actual measured surface settlement curve. However, due to the particularity of sandy cobble ground, the ground settlement lag caused by shield tunneling in this ground is extremely significant. As shown in Figure 6, when the shield cutter head is far away from the measuring point 5th to 11th, the settlement duration curve is a short section of the platform, followed by a sudden severe settlement. This is because the tunnel is disturbed by the shield to form a cavity, which can maintain stabilization itself within a certain period of time, but under the disturbance of the ground load, it gradually extends to the ground surface, causing an obvious collapse and also showing hysteresis.

The lag settlement process of ground surface is usually divided into different processes. The cobbles above the cutter head become loose and form a loose area. After the shield tunneling is overexcavated or shut down for a long time, the loose cobbles enter the soil. In the front and upper part of the cutter head, it causes ground loss and forms a cavity. However, due to the relatively large internal friction angle of the sandy cobble stratum, it has a certain arching effect, and the ground of the hemispherical dome is self-stable at this stage. Due to the rise of groundwater level, surface dynamic load, and other factors, the surface of self-stabilizing sandy cobble ground dome gradually peels off and develops to the surface. Finally, the ground penetrates to form a collapsed hole.

The occurrence of delayed settlement is mainly related to the special engineering geological properties of sandy cobble ground. Sandy cobble ground has large porosity, local formations sandwich lens sand layers, strong water permeability, and poor self-stability. Affected by the precipitation of surrounding structures along the shield tunnel and other factors, fine particles such as silt and fine sand in the ground

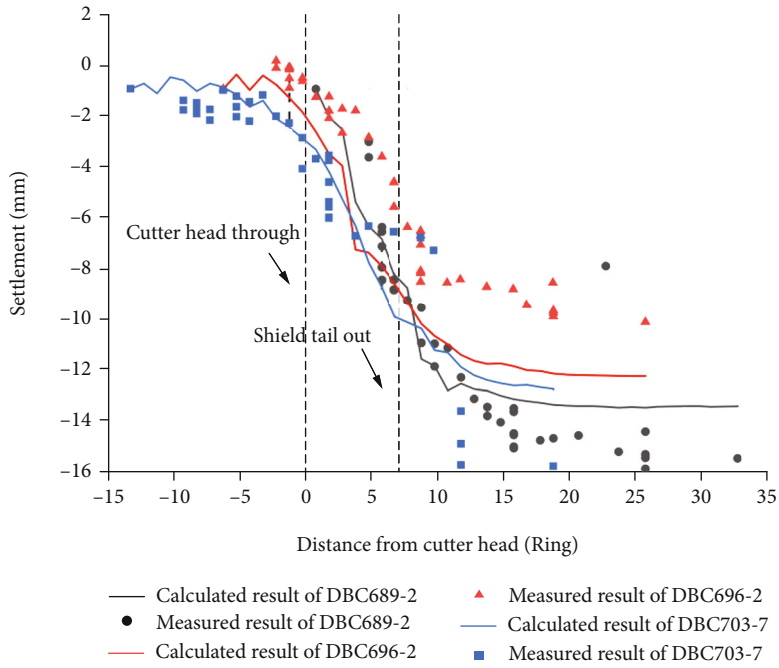

Figure 6: Comparison of settlement process.

are lost with the precipitation, resulting in a large gap between cobble particles, loose ground structure, and cobble skeleton structure. Under the influence of shield construction disturbance, the cobble skeleton is damaged, and a ground cavity with certain self-stabilizing ability is formed. Over a period of time, the ground cavity gradually developed and penetrated and eventually extended to the ground under the influence of groundwater coupling, ground load, construction disturbance, and other factors. The delayed settlement is extremely random, so the surface settlement result alone cannot fully reflect the ground loss, and it is impossible to predict the surface subsidence caused by the evolution of the cavity in the ground.

4.2. Ground Settlement. The ground settlement at the top of the tunnel increases with the increase of buried depth, and the settlement above the tunnel reaches the maximum value. The ground settlement below the tunnel decreases with the increase of buried depth, and the soil uplift at the bottom of the tunnel is the largest. Figure 7 shows the comparison of layered settlement of soil layer above the tunnel axis. From the simulation results in Figure 7(a), it can be seen that the difference in the layered settlement result at different depths before the shield tail is released. After the shield tail is released, the layered settlement gradually increases with the increase of the depth of the measuring point. The time history curve of layered settlement showed a downward trend as a whole, and the settlement increased significantly after the shield tail protruded. Due to the high sensitivity of the sandy cobble ground, the measured result fluctuates greatly, but the overall trend is the same, and both show a downward trend. The final settlement increases with the increase of the depth of the measuring point, indicating that the excavation amount of the shield machine is normal and the soil is not excessive. The body is only disturbed by the tunneling of the shield machine, and the measured result basically fluctuates around the simulated result. In Figure 7 (b), during the shield cutter head passes the 2nd and 5th rings of the measurement point, the layered settlement at 4.3 m below the ground suddenly increases. At this time, the amount of excavation in the tunnel is too large, forming a collapsed arch. A large cavity is formed above the tunnel. The ground settlement above the cavity increases suddenly, and the settlement in the cavity is difficult to detect. After this situation, no timely measures were taken, which caused the collapsed arch to be disturbed and destroyed after the cutter head passed the 10th ring of the measurement point, resulting in severe ground settlement.

From Figure 8(a), it can be seen that the time history curve of layered settlement at the depth of 1 m to 7 m shows a downward trend, and the layered settlement result gradually decreases with increasing the depth of the measuring point. The simulation results in Figure 8(b) show that the stratum settlement curve at 9 m-16 m shows an uplift trend, and the uplift amount increases with increasing the depth of the measuring point. Figure 8(a) shows the downward trend for the actual measured results of the 4 measuring points, which shows the upward trend. The overall trend is consistent with the simulation results. Nevertheless, it is worth noting that the measured results at 7.7 m and 9.7 m are significantly higher than those at other depths. The settlement first increases and then decreases from the surface to the ground. This may be due to the shield tunneling disturbance in water-rich sandy cobble ground. During the construction process, the silt and fine sand form a cavity in the middle of the ground due to piping and loss under the seepage action.

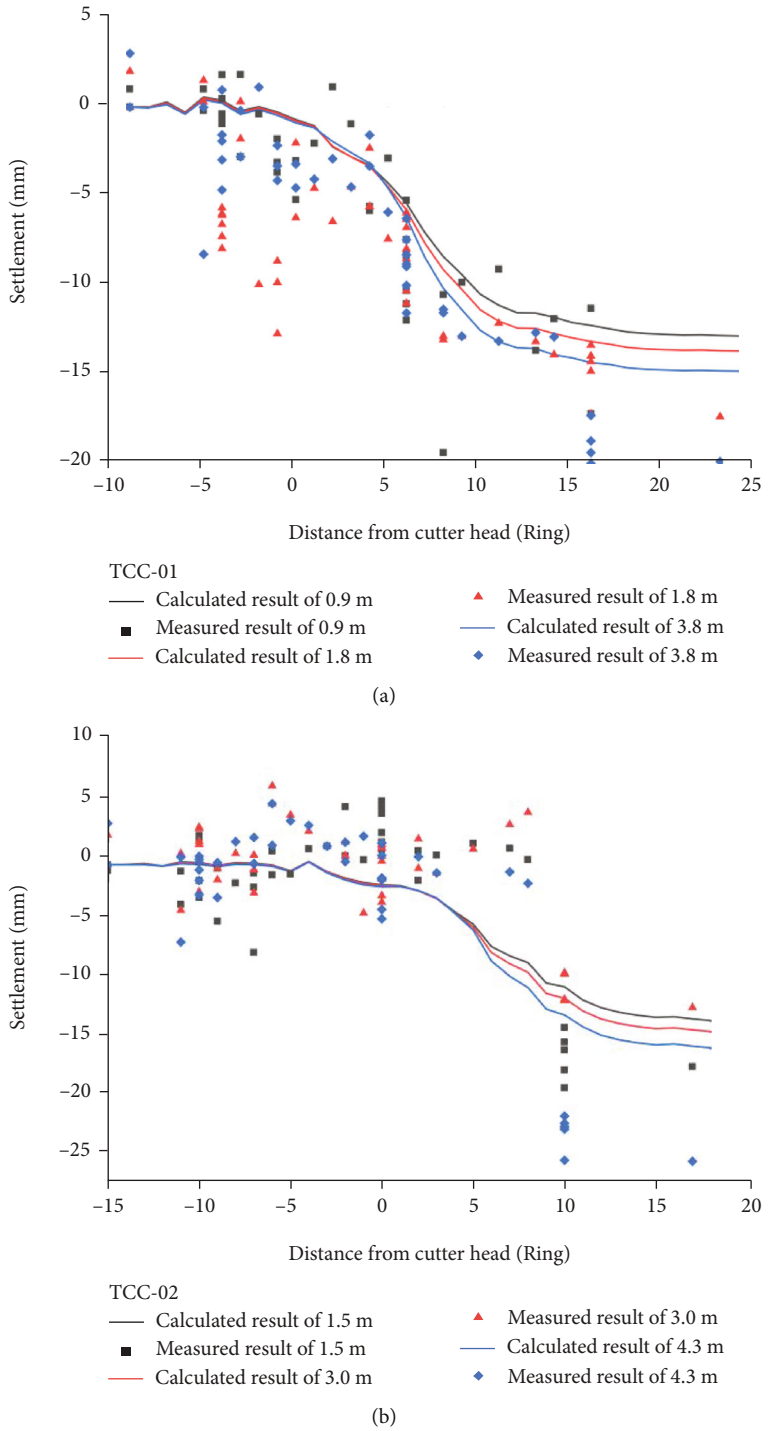

Figure 7: Settlement time history curve of soil layer above tunnel axis: (a) TCC-01 and (b) TCC-02.

The calculation results reveal the general law of the settlement in shield construction, but the sandy cobble ground has strong instability, and its instability mechanism is extremely complex. By comparing the monitoring and calculation results, we can find the abnormal conditions in the construction process, which is of great significance for timely implementing corresponding treatment measures during shield construction, preventing the continuous development of ground damage and avoiding collapse accidents.

4.3. Earth Pressure. Figure 9 shows that the simulated result of the incremental earth pressure at the positions 6 m and 8 m on both sides of the shield tunnel gradually decreases

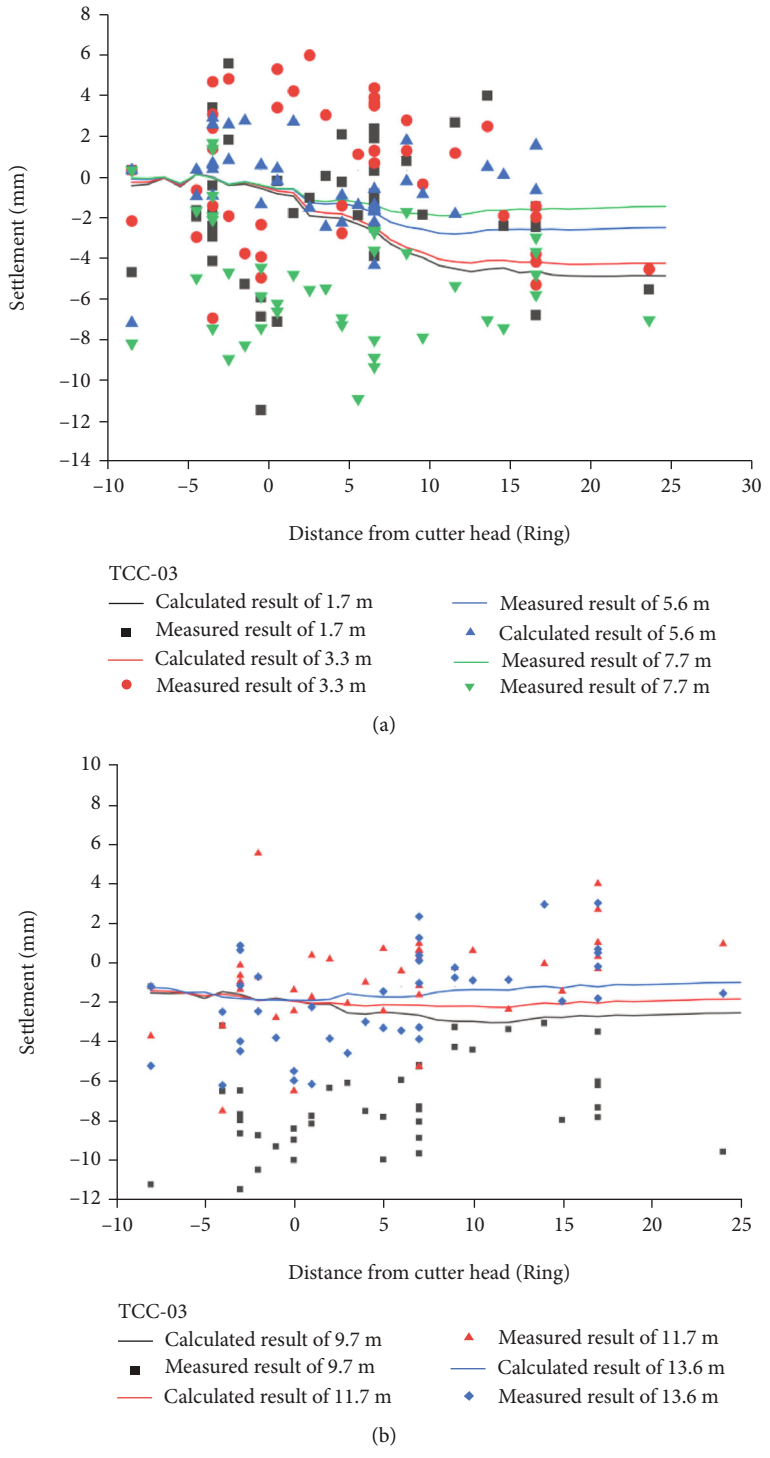

Figure 8: Comparison of time history curve of layered settlement at the center of two tunnels: (a) TCC-03 and (b) TCC-03.

with the excavation of the shield, and the incremental earth pressure at the measuring points at the depth of 10 m and 13 m gradually decreases with the excavation of shield. The earth pressure at the buried depth of 16 m decreases with the excavation. The sandy cobble ground is sensitive to stress, and the data fluctuates greatly. The variation range of longitudinal earth pressure increment on both sides of the shield tunnel is about 2 kPa, and the variation is very small. Apparently, the disturbance range of shield construction on sandy cobble ground is about twice the aperture.

Figure 10 depicts the variation of earth pressure increment at different depths of the tunnel centerline of D6. This shows that the increase of earth pressure at the buried depth measuring point at 6 m is small. The variation of the increase

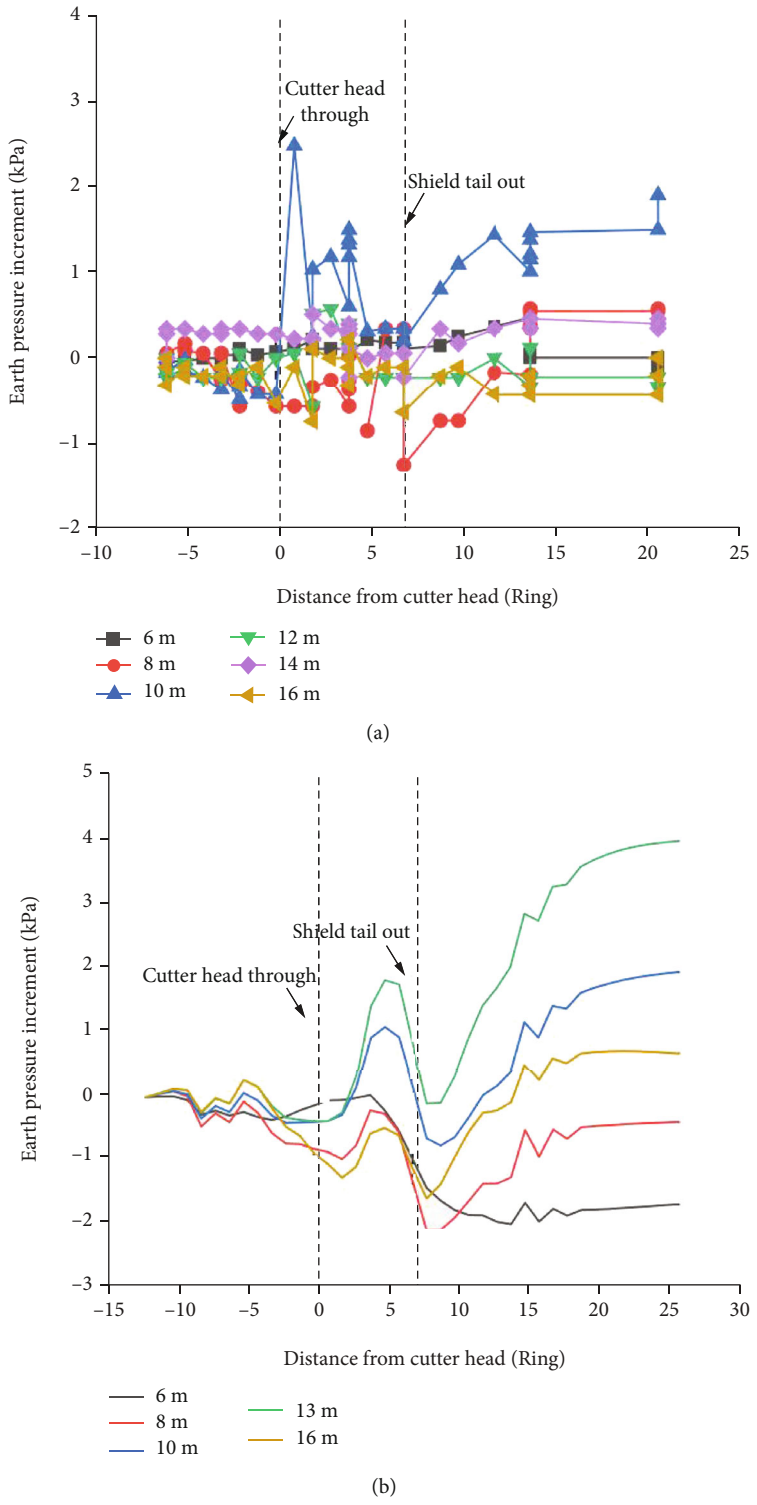

Figure 9: Time history curve of earth pressure of soil layer: (a) measured values and (b) calculation values.

of earth pressure at the buried depths of 8, 10, and 16 m can be divided into several stages. At first, the shield arrives at the front desk, and the increase of earth pressure is in the stage of slow increase. The cutter head reaches the first four rings of the section, i.e., about 6 m. When the cutter head reaches the section in the shield tunneling stage, the increase of earth pressure is affected by the support pressure on the excavation surface and decreases rapidly after reaching the extreme result. When the shield passes through the measuring point, the earth pressure fluctuates to a certain extent due to the disturbance of friction between the soil layer and the shield shell. This factor is not considered in the

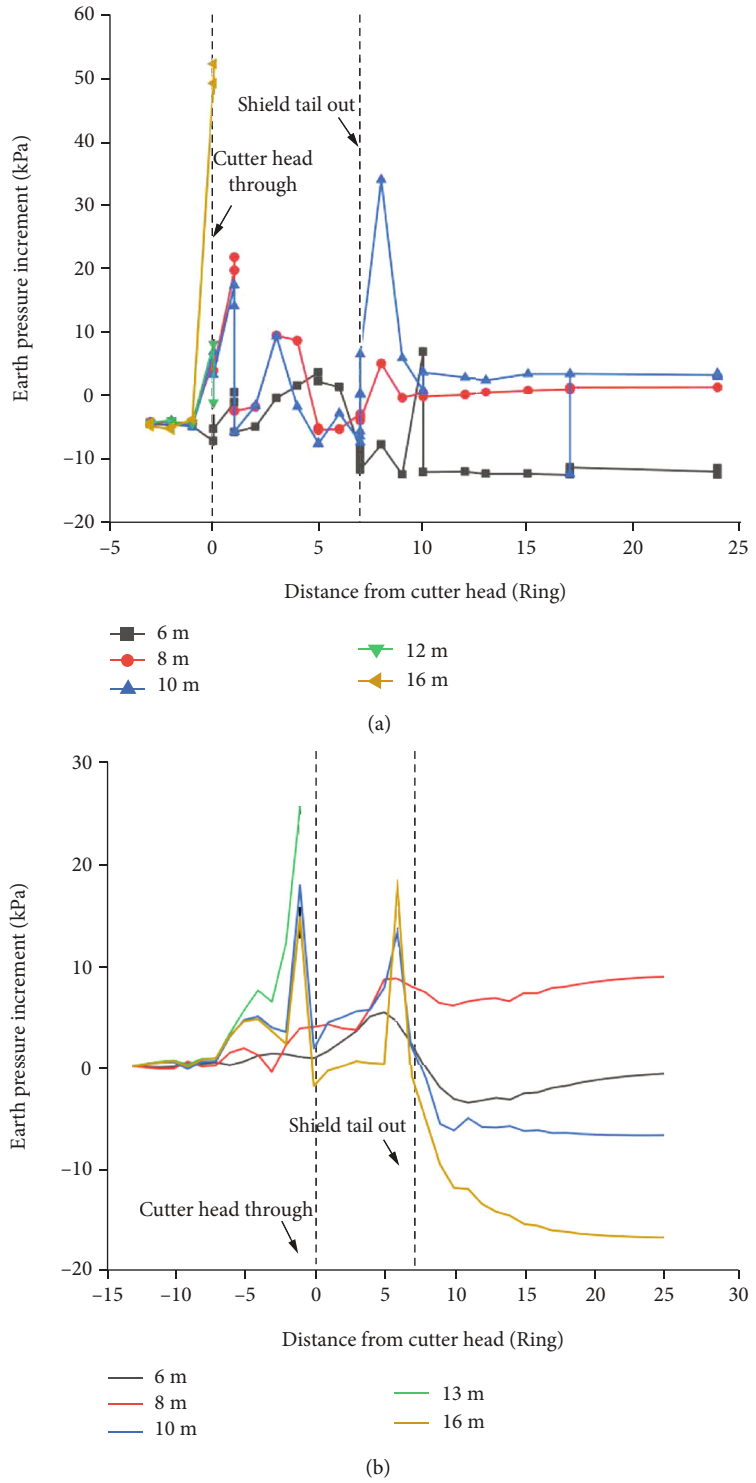

Figure 10: Earth pressure increment time history curve at different depths of tunnel centerline: (a) measured values and (b) calculation values.

simulation process of this model, so it is different from the measured data. When the shield tail reaches the measuring point, the earth pressure increment reaches the peak again due to the simultaneous grouting pressure. In the recovery stage, the earth pressure increment began to decrease after the shield tail was 6 m away from the section and then gradually stabilized. In addition, the earth pressure increases when the shield is driving dynamically. When the static section is assembled or closed, the earth pressure decreases. At the same time, due to the sensitive force of sandy cobble

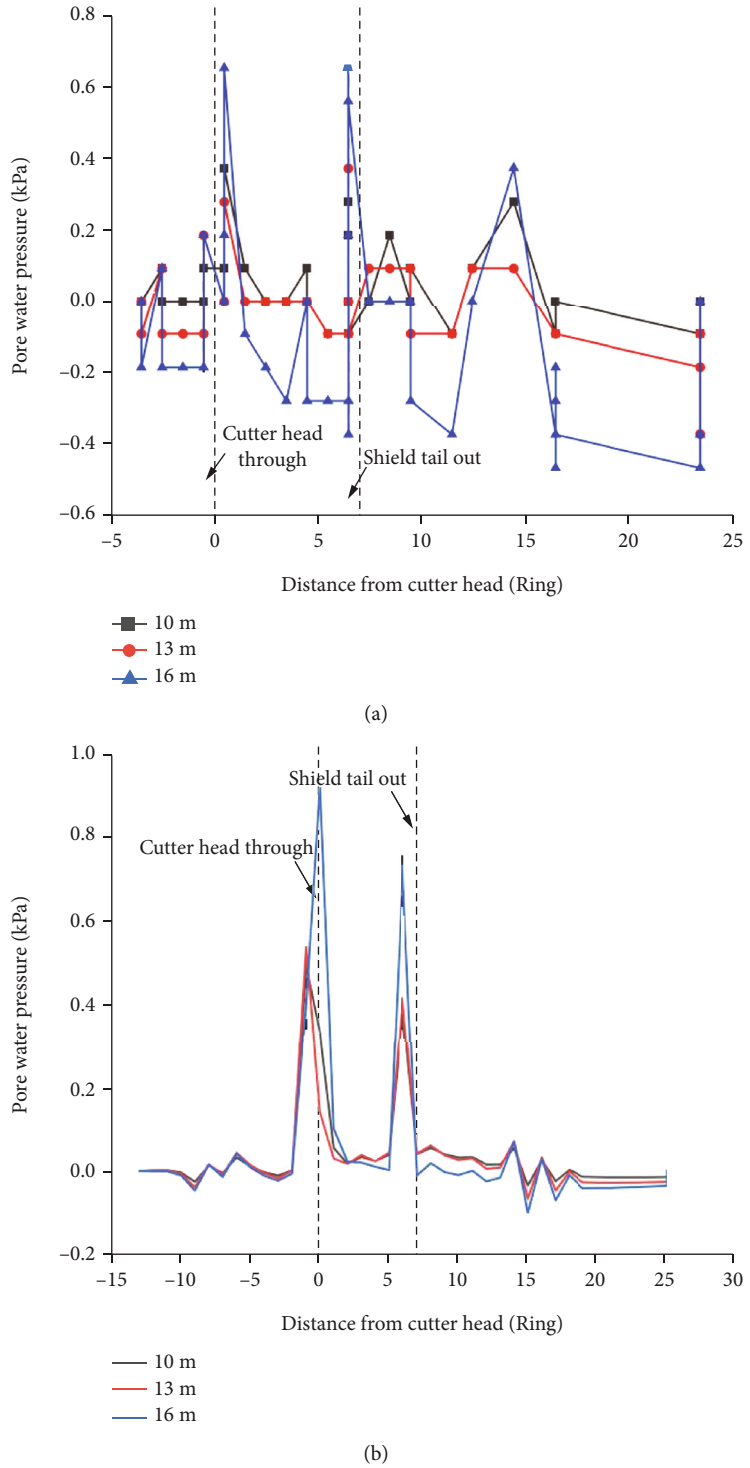

Figure 11: Excess pore water pressure time history curve at different buried depths of longitudinal lines on both sides of the tunnel: (a) measured values and (b) calculation values.

ground, the measured data fluctuates greatly, but the response time to disturbance is short.

4.4. Excess Pore Water Pressure. Figure 11 shows the variation of excess pore water pressure over time at the depths of 10, 13, and 16 m on both sides of the tunnel. At the position of transverse and longitudinal lines, there are two extreme results when the shield machine arrives and exits at the tail of the shield machine. Actually, the two extreme results are nearly the same. The results state clearly that the influence of the excavation surface support pressure on the excess pore water pressure of the soil layer near the

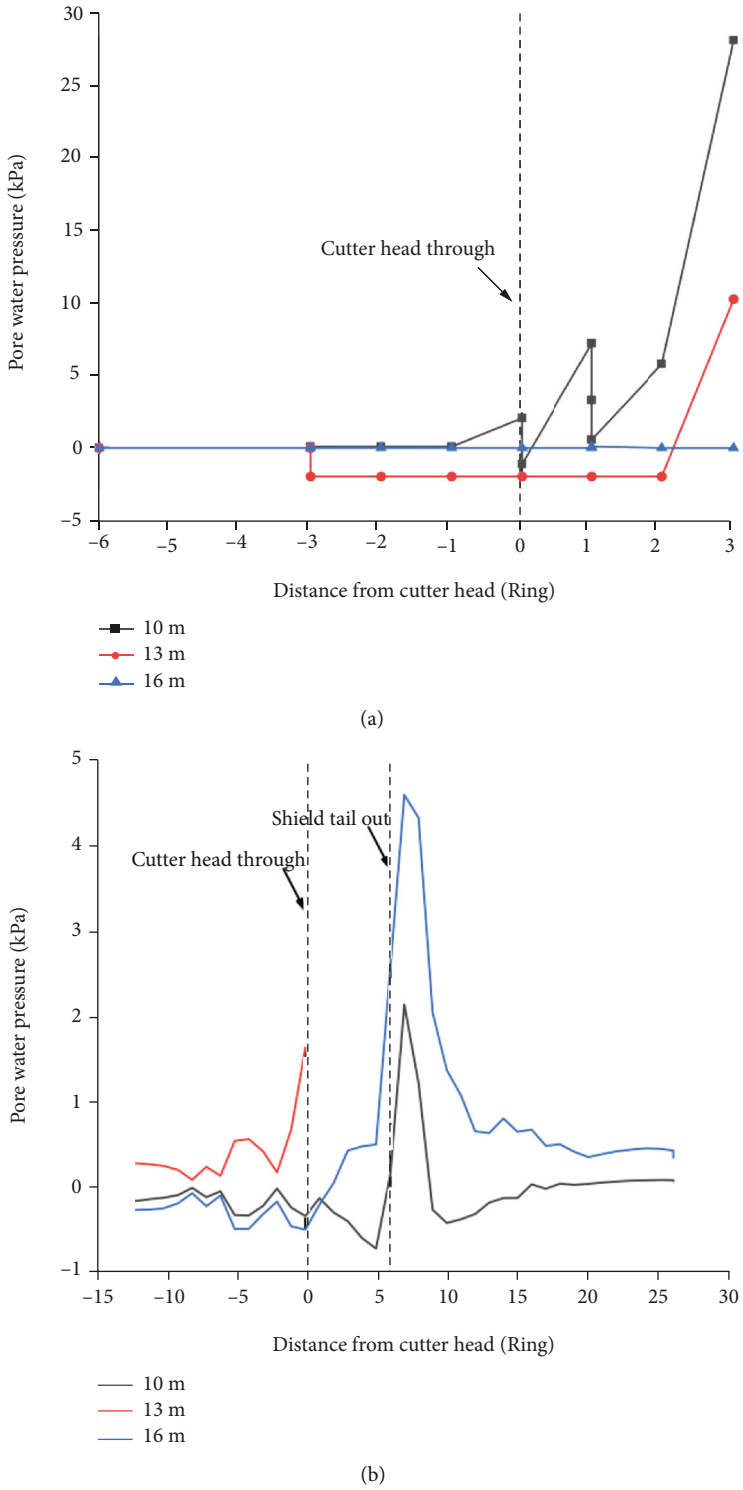

Figure 12: Excess pore water pressure time history curve at different buried depths of tunnel centerline: (a) measured values and (b) calculation values.

tunnel is the same as that of the grouting pressure. At the same time, the sandy cobble ground is highly permeable, the excess pore water pressure induced by the shield construction dissipates quickly, the data are different from clay layer, and the cumulative effect of excess pore water pressure is very small. The change of the longitudinal excess pore water pressure on both sides of the shield tunnel is very small. During shield tunnel construction in sandy cobble ground, the disturbance range of formation excess pore water pressure is about twice the tunnel diameter. It can be

found that when the shield passes through, the increase of excess pore water pressure at the center line of the tunnel reaches the maximum (Figure 12), and the change is much greater than the longitudinal line on both sides of the tunnel.

5. Conclusion

The width of the sedimentation trough of the sandy cobble ground is much narrower than that of the general clay and sandy soil layer. The maximum settlement result is basically consistent with that of the measured result. At the same time, the simulation results can simulate the five stages of normal settlement during shield construction, but cannot simulate the delayed settlement characteristic of sandy cobble ground.

By comparing the calculated results of layered settlement, the abnormal conditions in the construction process can be predicted in advance to a certain extent. The existence of cavities in the stratum is of great significance for the timely adoption of corresponding treatment measures to prevent the continuous development of ground damage.

The sandy cobble ground is sensitive to stress, and the responses of pore water pressure and earth pressure were very obvious. Actually, this process fluctuates greatly. The earth pressure and pore water pressure at the center line of the tunnel were significantly higher than the longitudinal lines on both sides of the tunnel; at this time, the earth pressure on the center line of the tunnel increases. The influence range of shield construction cross section is about twice the drilling radius, and the influence range of longitudinal section is about 6 m. The peak result is reached when the cutter head reaches and the shield tail exits.

Data Availability

The data used to support the findings of this study are available from the corresponding author upon request.

Conflicts of Interest

The authors Wang and Liu are employed by the China Hebei Construction and Geotechnical Investigation Group Ltd. All authors declare that there are no conflicts of interest regarding the publication of this manuscript.

Authors' Contributions

Wei Wang and Jingjing Liu have contributed to the conceptualization and methodology of the study. Xueming Zhang and Jing Chen have contributed to the investigation of the study.

Acknowledgments

Funding for this research was provided by the Hebei Province Postdoctoral Research Projects Merit-Based Funding Program (B2020005008).

References

[1] B. Bai, R. Zhou, G. Cai, W. Hu, and G. Yang, "Coupled thermo-hydro-mechanical mechanism in view of the soil particle rearrangement of granular thermodynamics," *Computers and Geotechnics*, vol. 137, no. 8, article 104272, 2021.

[2] B. Bai, G. C. Yang, T. Li, and G. S. Yang, "A thermodynamic constitutive model with temperature effect based on particle rearrangement for geomaterials," *Mechanics of Materials*, vol. 139, article 103180, 2019.

[3] L. Teng and H. Zhang, "Meso-macro analysis of surface settlement characteristics during shield tunneling in sandy cobble ground," *Rock and Soil Mechanics*, vol. 33, no. 4, pp. 1141–1150, 2012.

[4] P. Zhang, X. Du, D. Lu, L. Jin, and J. Qi, "Study on the excavation disturbed zone during tunneling in sandy cobble stratum considering the material meso-structure," *Transportation Geotechnics*, vol. 29, no. 4, article 100590, 2021.

[5] B. Bai, H. Li, T. Xu, and X. Chen, "Analytical solutions for contaminant transport in a semi-infinite porous medium using the source function method," *Computers and Geotechnics*, vol. 69, pp. 114–123, 2015.

[6] B. Bai and Z. Su, "Thermal responses of saturated silty clay during repeated heating-cooling processes," *Transport in Porous Media*, vol. 93, pp. 1–11, 2012.

[7] W. Hu, W. Cheng, S. Wen, and M. Rahman, "Effects of chemical contamination on microscale structural characteristics of intact loess and resultant macroscale mechanical properties," *Catena*, vol. 203, article 105361, 2021.

[8] B. Bai, Q. Nie, Y. Zhang, X. Wang, and W. Hu, "Cotransport of heavy metals and SiO_2 particles at different temperatures by seepage," *Journal of Hydrology*, vol. 597, article 125771, 2021.

[9] B. Bai, T. Xu, Q. Nie, and P. Li, "Temperature-driven migration of heavy metal Pb^{2+} along with moisture movement in unsaturated soils," *International Journal of Heat and Mass Transfer*, vol. 153, article 119573, 2020.

[10] J. Fan, F. Yong, X. Zhang, and Z. Yang, "Ground movement induced by shield tunnel construction in sandy cobble stratum," *Chinese Journal of Underground Space and Engineering*, vol. 13, no. 6, pp. 1599–1607, 2017.

[11] Y. Jiang, Y. Fang, C. He, and J. Wang, "Study on delayed settlement formation induced by shield tunneling in sandy cobble strata," *Chinese Journal of Underground Space and Engineering*, vol. 11, no. 1, pp. 171–177, 2015.

[12] Q. Yao, H. Di, C. Ji, and S. Zhou, "Ground collapse caused by shield tunneling in sandy cobble stratum and its control measures," *Bulletin of Engineering Geology and the Environment*, vol. 79, no. 10, pp. 5599–5614, 2020.

[13] X. Yang, "Study on boring parameters of composite EPB shield in sandy cobble strata and study on ground deformation rule," *Tunnel Construction*, vol. 34, no. 8, pp. 721–730, 2014.

[14] L. Zhang, S. Yang, and J. Guo, "Key technology of earth pressure balance shield construction in water-rich sandy gravel stratum," *Tunnel Construction*, vol. 29, no. S1, pp. 52–56, 2009.

[15] W. Hu, C. Wen-Chieh, S. Wen, and K. Yuan, "Revealing enhancement and degradation mechanisms affecting calcite precipitation in EICP process," *Frontiers in Bioengineering and Biotechnology*, vol. 9, article 750258, 2021.

[16] B. Yuan, Z. Li, Z. Zhao, H. Ni, Z. Su, and Z. Li, "Experimental study of displacement field of layered soils surrounding

laterally loaded pile based on transparent soil," *Journal of Soils and Sediments*, vol. 21, no. 9, pp. 3072–3083, 2021.

[17] B. Yuan, Z. Li, W. Chen et al., "Influence of groundwater depth on pile–soil mechanical properties and fractal characteristics under cyclic loading," *Fractal and Fractional*, vol. 6, no. 4, p. 198, 2022.

[18] C. Cui, K. Meng, C. Xu, Z. Liang, H. Li, and H. Pei, "Analytical solution for longitudinal vibration of a floating pile in saturated porous media based on a fictitious saturated soil pile model," *Computers and Geotechnics*, vol. 131, article 103942, 2021.

[19] B. Bai and T. Li, "Irreversible consolidation problem of a saturated porothermoelastic spherical body with a spherical cavity," *Applied Mathematical Modelling*, vol. 37, no. 4, pp. 1973–1982, 2013.

[20] B. Bai, Y. Wang, D. Rao, and F. Bai, "The effective thermal conductivity of unsaturated porous media deduced by pore-scale SPH simulation," *Frontiers in Earth Science*, 2022.

[21] B. Yuan, Z. Li, Y. Chen et al., "Mechanical and microstructural properties of recycling granite residual soil reinforced with glass fiber and liquid-modified polyvinyl alcohol polymer," *Chemosphere*, vol. 268, article 131652, 2022.

[22] B. Bai, F. Long, D. Rao, and T. Xu, "The effect of temperature on the seepage transport of suspended particles in a porous medium," *Hydrological Processes*, vol. 31, no. 2, pp. 382–393, 2017.

[23] X. D. Fu, Q. Sheng, Y. H. Zhang, J. Chen, S. K. Zhang, and Z. P. Zhang, "Computation of the safety factor for slope stability using discontinuous deformation analysis and the vector sum method," *Computers and Geotechnics*, vol. 92, pp. 68–76, 2017.

[24] Z. Xue, W. Cheng, L. Wang, and G. Song, "Improvement of the shearing behaviour of loess using recycled straw fiber reinforcement," *KSCE Journal of Civil Engineering*, vol. 25, no. 9, pp. 3319–3335, 2021.

[25] B. Bai, D. Rao, T. Xu, and P. Chen, "SPH-FDM boundary for the analysis of thermal process in homogeneous media with a discontinuous interface," *International Journal of Heat and Mass Transfer*, vol. 117, pp. 517–526, 2018.

[26] B. Bai and X. Shi, "Experimental study on the consolidation of saturated silty clay subjected to cyclic thermal loading," *Geomechanics and Engineering*, vol. 12, no. 4, pp. 707–721, 2017.

[27] Z. F. Xue, W. C. Cheng, L. Wang, and W. Hu, "Effects of bacterial inoculation and calcium source on microbial-induced carbonate precipitation for lead remediation," *Journal of Hazardous Materials*, vol. 426, article 128090, 2021.

[28] G. C. Yang and B. Bai, "Thermo-hydro-mechanical model for unsaturated clay soils based on granular solid hydrodynamics theory," *International Journal of Geomechanics*, vol. 19, no. 10, 2019.

[29] B. Bai, L. Guo, and S. Han, "Pore pressure and consolidation of saturated silty clay induced by progressively heating/cooling," *Mechanics of Materials*, vol. 75, pp. 84–94, 2014.

[30] A. Khabbazi, M. Ghafoori, S. Tarighazali, and A. Cheshomi, "Experimental and laboratory assessment of clogging potential based on adhesion," *Bulletin of Engineering Geology and the Environment*, vol. 78, no. 1, pp. 605–616, 2019.

[31] Z. Zizka, B. Schoesser, M. Thewes, and T. Schanz, "Slurry shield tunneling: new methodology for simplified prediction of increased pore pressures resulting from slurry infiltration at the tunnel face under cyclic excavation processes," *International Journal of Civil Engineering*, vol. 17, no. 1, pp. 113–130, 2019.

[32] A. Hamrouni, D. Dias, and B. Sbartai, "Probability analysis of shallow circular tunnels in homogeneous soil using the surface response methodology optimized by a genetic algorithm," *Tunnelling and Underground Space Technology*, vol. 86, pp. 22–33, 2019.

[33] E. Gholizadeh and M. Latifi, "A coupled hydro-mechanical constitutive model for unsaturated frictional and cohesive soil," *Computers and Geotechnics*, vol. 98, pp. 69–81, 2018.

[34] A. Deganutti, P. Tecca, and R. Genevois, "The measure of friction angles for different types of granular material," *Journal of Mountain Science*, vol. 16, no. 4, pp. 769–777, 2019.

[35] M. Aslani, J. Nazariafshar, and N. Ganjian, "Experimental study on shear strength of cohesive soils reinforced with stone Columns," *Geotechnical and Geological Engineering*, vol. 37, no. 3, pp. 2165–2188, 2019.

[36] B. Xue-Dong, C. Wen-Chieh, and L. Ge, "A comparative study of different machine learning algorithms in predicting EPB shield behaviour: a case study at the Xi'an metro, China," *Acta Geotechnica*, vol. 16, no. 12, pp. 4061–4080, 2021.

[37] X. Bai, W. Cheng, B. Sheil Brian, and G. Li, "Pipejacking clogging detection in soft alluvial deposits using machine learning algorithms," *Tunnelling and Underground Space Technology*, vol. 113, article 103908, 2021.

[38] B. Bai, "Fluctuation responses of saturated porous media subjected to cyclic thermal loading," *Computers and Geotechnics*, vol. 33, no. 8, pp. 396–403, 2006.

[39] H. Sohaei, M. Hajihassani, E. Namazi, and A. Marto, "Experimental study of surface failure induced by tunnel construction in sand," *Engineering Failure Analysis*, vol. 118, article 104897, 2020.

[40] Y. Q. Zhou, Q. Sheng, N. N. Li, and X. D. Fu, "The dynamic mechanical properties of a hard rock under true triaxial damage-controlled dynamic cyclic loading with different loading rates: a case study," *Rock Mechanics and Rock Engineering*, vol. 55, no. 4, pp. 2471–2492, 2022.

[41] M. Zhang, R. Xu, and J. H. Guo, "Liquefaction discrimination of the coastal stratum of lligan in China code and NCEER method," *Fresenius Environmental Bulletin*, vol. 31, pp. 1495–1502, 2022.

[42] X. D. Fu, Q. Sheng, G. Li, Z. Zhang, Y. Zhou, and Y. Du, "Analysis of landslide stability under seismic action and subsequent rainfall: a case study on the Ganjiazhai giant landslide along the Zhaotong-Qiaojia road during the 2014 Ludian earthquake, Yunnan, China," *Bulletin of Engineering Geology and the Environment*, vol. 79, no. 10, pp. 5229–5248, 2020.